Lattice Boltzmann Method for Fluid Simulations

Technical Report · April 2014

CITATIONS
45

READS
9,974

2 authors, including:

Yuanxun Bao
New York University
7 PUBLICATIONS **137** CITATIONS

Lattice Boltzmann Method for Fluid Simulations

Yuanxun Bill Bao & Justin Meskas

April 14, 2011

1 Introduction

In the last two decades, the Lattice Boltzmann method (LBM) has emerged as a promising tool for modelling the Navier-Stokes equations and simulating complex fluid flows. LBM is based on microscopic models and mesoscopic kinetic equations. In some perspective, it can be viewed as a finite difference method for solving the Boltzmann transport equation. Moreover the Navier-Stokes equations can be recovered by LBM with a proper choice of the collision operator. In Section 2 and 3, we first introduce this method and describe some commonly used boundary conditions. In Section 4, the validity of this method is confirmed by comparing the numerical solution to the exact solution of the steady plane Poiseuille flow and convergence of solution is established. Some interesting numerical simulations, including the lid-driven cavity flow, flow past a circular cylinder and the Rayleigh-Bénard convection for a range of Reynolds numbers, are carried out in Section 5, 6 and 7. In Section 8, we briefly highlight the procedure of recovering the Navier-Stokes equations from LBM. A summary is provided in Section 9.

2 Lattice Boltzmann Model

The Lattice Boltzmann method [1, 2, 3] was originated from Ludwig Boltzmann's kinetic theory of gases. The fundamental idea is that gases/fluids can be imagined as consisting of a large number of small particles moving with random motions. The exchange of momentum and energy is achieved through particle streaming and billiard-like particle collision. This process can be modelled by the Boltzmann transport equation, which is

$$\frac{\partial f}{\partial t} + \vec{u} \cdot \nabla f \quad = \quad \Omega \tag{1}$$

where $f(\vec{x}, t)$ is the particle distribution function, $\vec{u}$ is the particle velocity, and Ω is the collision operator. The LBM simplifies Boltzmann's original idea of gas dynamics by reducing the number of particles and confining them to the nodes of a lattice. For a two dimensional model, a particle is restricted to stream in a possible of 9 directions, including the one staying at rest. These velocities are referred to as the *microscopic velocities* and denoted by $\vec{e}_i$, where $i = 0, \ldots, 8$. This model is commonly known as the D2Q9 model as it is two dimensional and involves 9 velocity vectors. Figure 1 shows a typical lattice node of D2Q9 model with 9 velocities $\vec{e}_i$ defined by

$$\vec{e}_i \quad = \quad \begin{cases} (0,0) & i = 0 \\ (1,0), (0,1), (-1,0), (0,-1) & i = 1,2,3,4 \\ (1,1), (-1,1), (-1,-1), (1,-1) & i = 5,6,7,8 \end{cases} \tag{2}$$

For each particle on the lattice, we associate a discrete probability distribution function $f_i(\vec{x}, \vec{e}_i, t)$ or simply $f_i(\vec{x}, t)$, $i = 0 \ldots 8$, which describes the probability of streaming in one particular direction.

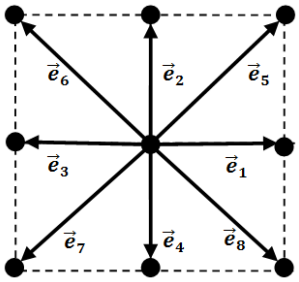

Figure 1: Illustration of a lattice node of the D2Q9 model

The *macroscopic fluid density* can be defined as a summation of microscopic particle distribution function,

$$\rho(\vec{x},t) \quad = \quad \sum_{i=0}^{8} f_i(\vec{x},t) \tag{3}$$

Accordingly, the *macroscopic velocity* $\vec{u}(\vec{x},t)$ is an average of microscopic velocities $\vec{e}_i$ weighted by the distribution functions f_i,

$$\vec{u}(\vec{x},t) \quad = \quad \frac{1}{\rho}\sum_{i=0}^{8} c f_i \vec{e}_i \tag{4}$$

The key steps in LBM are the streaming and collision processes which are given by

$$\underbrace{f_i(\vec{x}+c\vec{e}_i\Delta t, t+\Delta t) - f_i(\vec{x},t)}_{\text{Streaming}} \quad = \quad \underbrace{-\frac{[f_i(\vec{x},t) - f_i^{eq}(\vec{x},t)]}{\tau}}_{\text{Collision}} \tag{5}$$

In the actual implementation of the model, streaming and collision are computed separately, and special attention is given to these when dealing with boundary lattice nodes. Figure 2 shows graphically how the streaming step takes place for the interior nodes.

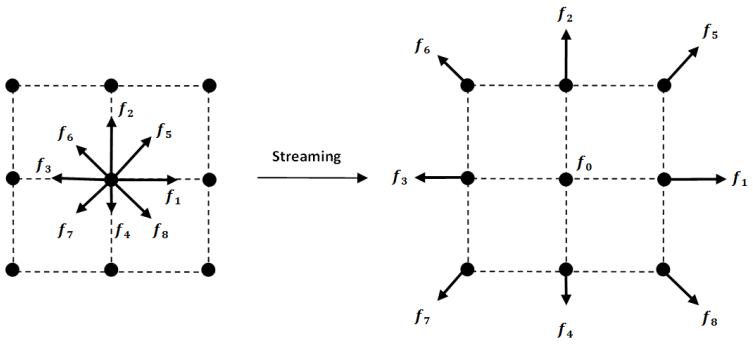

Figure 2: Illustration of the streaming process of a lattice node

In the collision term of (5), $f_i^{eq}(\vec{x},t)$ is the equilibrium distribution, and τ is considered as the relaxation time towards local equilibrium. For simulating single phase flows, it suffices to use Bhatnagar-Gross-Krook (BGK) collision, whose equilibrium distribution f_i^{eq} is defined by

$$f_i^{eq}(\vec{x},t) \quad = \quad w_i\rho + \rho s_i(\vec{u}(\vec{x},t)) \tag{6}$$

where $s_i(\vec{u})$ is defined as

$$s_i(\vec{u}) = w_i \left[3\frac{\vec{e}_i \cdot \vec{u}}{c} + \frac{9}{2}\frac{(\vec{e}_i \cdot \vec{u})^2}{c^2} - \frac{3}{2}\frac{\vec{u} \cdot \vec{u}}{c^2} \right], \tag{7}$$

and w_i, the weights,

$$w_i = \begin{cases} 4/9 & i = 0 \\ 1/9 & i = 1, 2, 3, 4 \\ 1/36 & i = 5, 6, 7, 8 \end{cases} \tag{8}$$

and $c = \dfrac{\Delta x}{\Delta t}$ is the lattice speed. The fluid kinematic viscosity ν in the D2Q9 model is related to the relaxation time τ by

$$\nu = \frac{2\tau - 1}{6}\frac{(\Delta x)^2}{\Delta t} \tag{9}$$

The algorithm can be summarized as follows:

1. Initialize ρ, $\vec{u}$, f_i and f_i^{eq}
2. Streaming step: move $f_i \longrightarrow f_i^*$ in the direction of $\vec{e_i}$
3. Compute macroscopic ρ and $\vec{u}$ from f_i^* using (3) and (4)
4. Compute f_i^{eq} using (6)
5. Collision step: calculate the updated distribution function $f_i = f_i^* - \dfrac{1}{\tau}(f_i^* - f_i^{eq})$ using (5)
6. Repeat step 2 to 5

Notice that numerical issues can arise as $\tau \to 1/2$. During the streaming and collision step, the boundary nodes require some special treatments on the distribution functions in order to satisfy the imposed macroscopic boundary conditions. We discuss these in details in Section 3.

3 Boundary Conditions

Boundary conditions (BCs) are central to the stability and the accuracy of any numerical solution. For the lattice Boltzmann method, the discrete distribution functions on the boundary have to be taken care of to reflect the macroscopic BCs of the fluid. In this project, we explore two of the most widely used BCs: Bounce-back BCs [4] and Zou-He velocity and pressure (density) BCs [5].

3.1 Bounce-back BCs

Bounce-back BCs are typically used to implement no-slip conditions on the boundary. By the so-called bounce-back we mean that when a fluid particle (discrete distribution function) reaches a boundary node, the particle will scatter back to the fluid along with its incoming direction. Bounce-back BCs come in a few variants and we focus on two types of implementations: the on-grid and the mid-grid bounce-back [4].

The idea of the on-grid bounce-back is particularly simple and preserves a decent numerical accuracy. In this configuration, the boundary of the fluid domain is aligned with the lattice points (see Figure 3). One can use a boolean mask for the boundary and the interior nodes. The incoming directions of the distribution functions are reversed when encountering a boundary node. This implementation

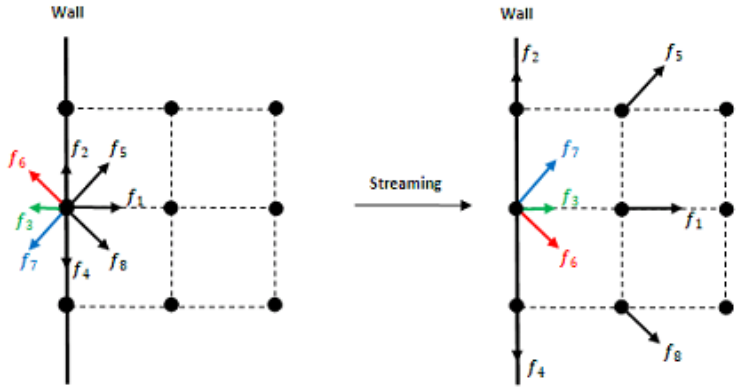

Figure 3: Illustration of on-grid bounce-back

does not distinguish the orientation of the boundaries and is ideal for simulating fluid flows in complex geometries, such as the porous media flow.

The configuration of the mid-grid bounce-back introduces fictitious nodes and places the boundary wall centered between fictitious nodes and boundary nodes of the fluid (see Figure 4). At a given time step t, the distribution functions with directions towards the boundary wall would leave the domain. Collision process is then applied and directions of these distribution functions are reversed and they bounce back to the boundary nodes. We point out that the distribution functions at the end of bounce-back in this configuration is the post-collision distribution functions.

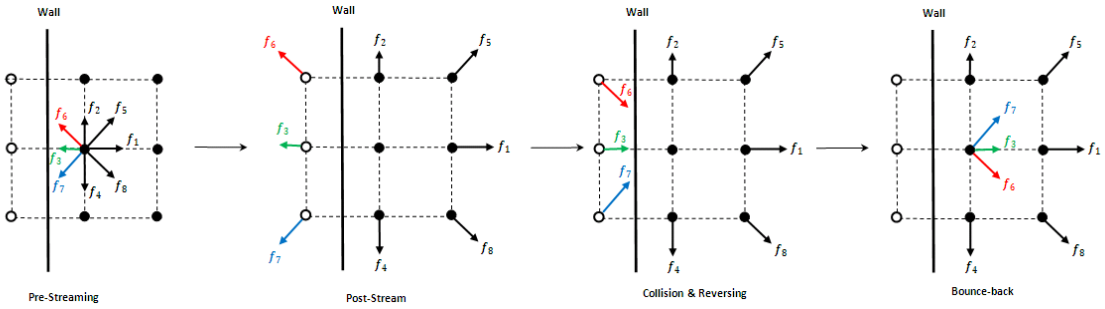

Figure 4: Illustration of mid-grid bounce-back

Although the on-grid bounce-back is easy to implement, it has been verified that it is only first-order accurate due to its one-sided treatment on streaming at the boundary. However the centered nature of the mid-grid bounce-back leads to a second order of accuracy at the price of a modest complication.

3.2 Zou-He Velocity and Pressure BCs

In many physical situations, we would like to model flows with prescribed velocity or pressure (density) at the boundary. This particular velocity/pressure BC we discuss here was originally developed by Zou and He in [5]. For illustration, we consider that the velocity $\vec{u}_L = (u, v)$ is given on the left boundary. After streaming, f_0, f_2, f_3, f_4, f_6 and f_7 are known. What's left undetermined are f_1, f_5, f_8 and ρ (see Figure 5).

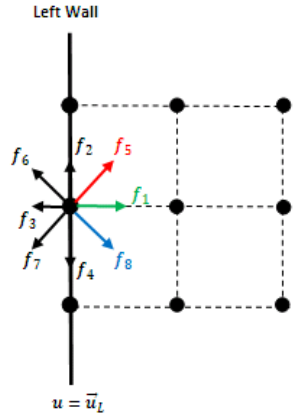

Figure 5: Illustration of Zou-He velocity BC

The idea of Zou-He BCs is to formulate a linear system of f_1, f_5, f_8 and ρ using (3) and (4). After rearranging:

$$\begin{aligned} f_1 + f_5 + f_8 &= \rho - (f_0 + f_2 + f_4 + f_3 + f_6 + f_7) && (10) \\ f_1 + f_5 + f_8 &= \rho u + (f_3 + f_6 + f_7) && (11) \\ f_5 - f_8 &= \rho v - f_2 + f_4 - f_6 + f_7 && (12) \end{aligned}$$

By considering (10) and (11), we can determine

$$\rho = \frac{1}{1-u}\left[(f_0 + f_2 + f_4 + 2(f_3 + f_6 + f_7)\right] \quad (13)$$

However, we need a fourth equation to close the system and solve for f_1, f_5 and f_8. The assumption made by Zou and He is that the bounce-back rule still holds for the non-equilibrium part of the particle distribution normal to the boundary. In this case, the fourth equation is

$$f_1 - f_1^{eq} = f_3 - f_3^{eq} \quad (14)$$

With f_1 solved by (6) and (14), f_5, f_8 are subsequently determined:

$$\begin{aligned} f_1 &= f_3 + \frac{2}{3}\rho v && (15) \\ f_5 &= f_7 - \frac{1}{2}(f_2 - f_4) + \frac{1}{6}\rho u + \frac{1}{2}\rho v && (16) \\ f_8 &= f_6 + \frac{1}{2}(f_2 - f_4) + \frac{1}{6}\rho u - \frac{1}{2}\rho v && (17) \end{aligned}$$

A similar procedure is taken if a given pressure (density) is imposed on the boundary. Here we notice that this type of BC depends on the orientation of the boundary and thus is hard to generalize for complex geometries.

4 Steady Plane Poiseuille Flow

In this simulation we apply the lattice BGK model in Section 2 to solve the steady plane Poiseuille flow. The flow is steady and in driven by a pressure gradient at the inlet and the outlet of the channel (see Figure 6).

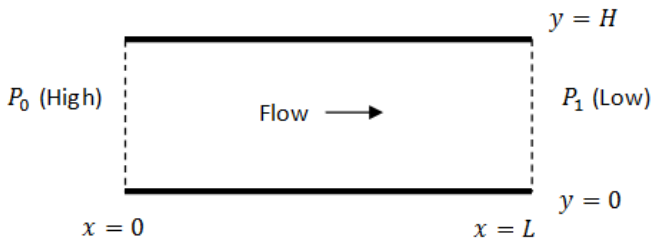

Figure 6: Plane Poiseuille flow

By using symmetry and incompressibility, the velocity components u, v do not have any horizontal variation and $v \equiv 0$. The Navier-Stokes equations are further reduced to

$$\mu \frac{\partial^2 u}{\partial y^2} = \frac{\partial p}{\partial x}, \tag{18}$$

where $\dfrac{\partial p}{\partial x} = \dfrac{P_1 - P_0}{L}$. The initial and boundary conditions are

$$\begin{aligned} u(x,y,0) = v(x,y,0) = 0; \qquad & p(x,y,0) = P_{avg} \\ u(x,0,t) = v(x,0,t) = 0; \qquad & u(x,H,t) = v(x,H,t) = 0 \\ p(0,y,t) = P_0; \qquad & p(L,y,t) = P_1 \end{aligned}$$

where $P_{avg} = (P_0 + P_1)/2$, and P_0 and P_1 are the pressure at the inlet and the outlet of the channel. The steady Poiseuille flow has the exact solution for velocity:

$$u(x,y,t) = \frac{\Delta p}{2\mu L} y(y - H) \tag{19}$$

$$v(x,y,t) = 0 \tag{20}$$

For the simulation, we apply periodic BCs at the inlet and the outlet. Both mid-grid and on-grid BCs are implemented on the top and bottom plates and compared for convergence. We take $L = 40$, $H = 32$, $\Delta p = -0.05$, $\tau = 1$. The criterion of steady state is

$$\frac{\sum_{ij} |u_{ij}^{n+1} - u_{ij}^{n}|}{\sum_{ij} |u_{ij}^{n+1}|} \leq 5.0 \times 10^{-9} \tag{21}$$

where u_{ij}^{n} is the horizontal velocity component on (x_i, y_j) at the n^{th} time step.

The left graph of Figure 7 shows that the computed velocity profile agrees closely with the analytical solution. The first order convergence of on-grid bounce-back and the second order convergence of mid-grid bounce-back, discussed in Section 3.1, have been validated for this problem in the convergence plot.

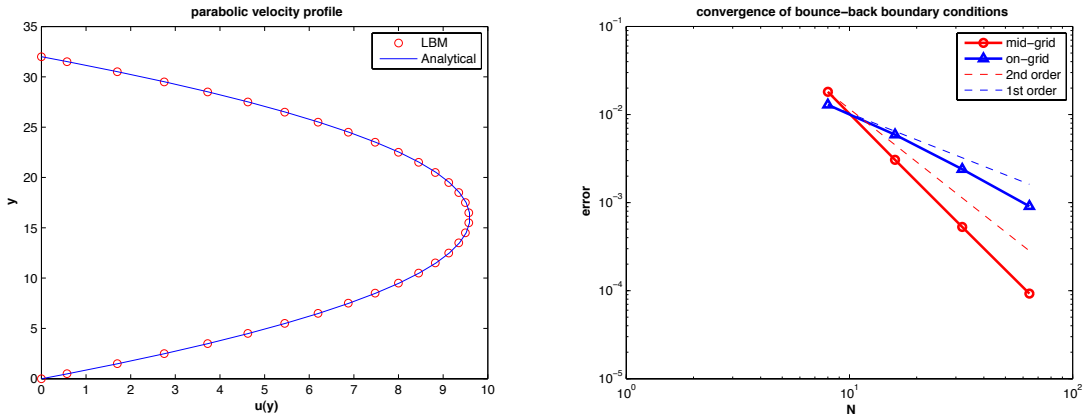

Figure 7: Parabolic velocity profile of plane Poiseuille flow and convergence of solution

5 Lid-Driven Cavity Flow

In this simulation we have a 2D fluid flow that is driven by a lid at the top which moves at a speed of $\vec{u}(\vec{x}, 1, t) = V_d$ in the right direction. The other three walls have bounce-back BCs for the distribution function and no-slip BCs for the velocity, $u = 0$ and $v = 0$. The moving lid has Zou-He BCs . The initial conditions state that the velocity field is zero everywhere and the initial distribution function is set by the weights, $f_i = w_i$. This results in an initial condition that $\rho = 1$ from (3). The only exception is the velocity of the fluid on the top is set to be V_d.

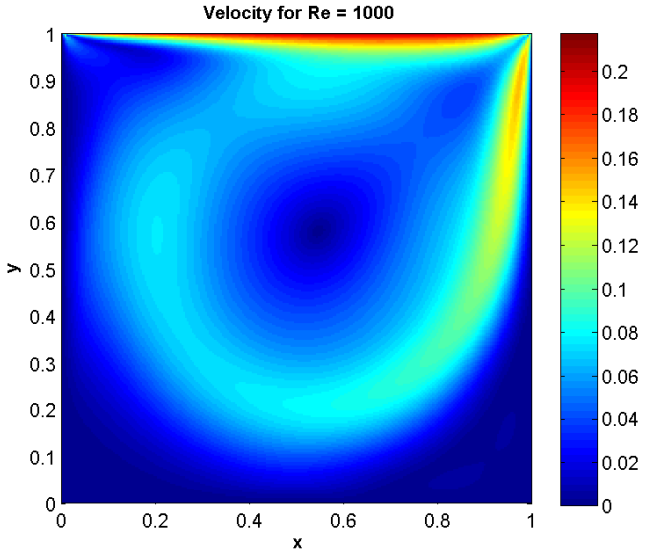

Figure 8: Color plot of the norm of the velocity: $Re = 1000$, $\nu = 1/18$, $\tau = 2/3$, 256×256 lattice

The two top corner lattice points are singular points and are considered as part of the moving lid. Simulations were done with a 256×256 lattice, $\nu = 1/18$, $\tau = 2/3$ and with $Re = 400$ and 1000. Figure 8 shows a color visualization of the simulation for $Re = 1000$.

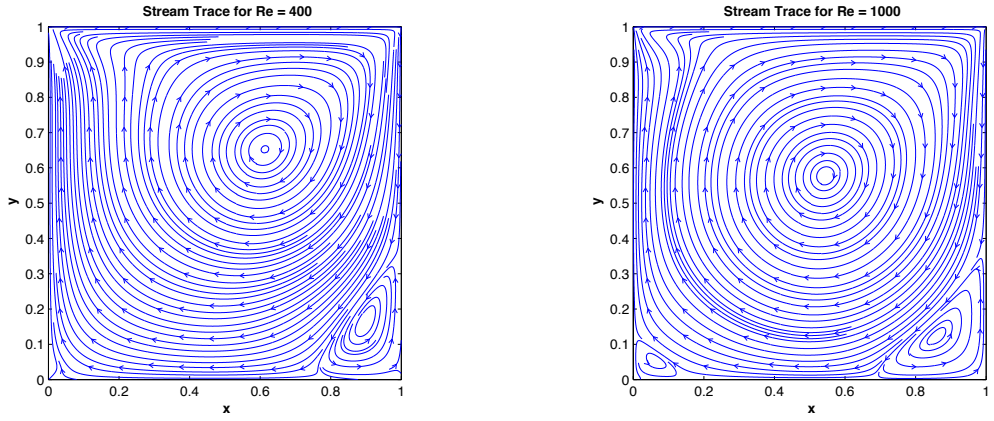

Figure 9: Stream traces for $Re = 400$ and 1000, $\nu = 1/18$, $\tau = 2/3$, 256×256 lattice

From the stream traces of Figure 9 the simulation produces similar vortex-like behavior as a real physical flow, with a clockwise center vortex and a counter-clockwise secondary vortex in the right bottom corner. With higher Re a third counter-clockwise vortex is visible in the left bottom corner.

6 Flow Past A Circular Cylinder

The study of flow past an object dates its history back to aircraft design in the early 20th century. Researchers were interested in the design of wings of an aircraft and understanding the behavior of the flow past them. It turns out that the Reynolds number plays an important role in characterizing the behavior of the flow.

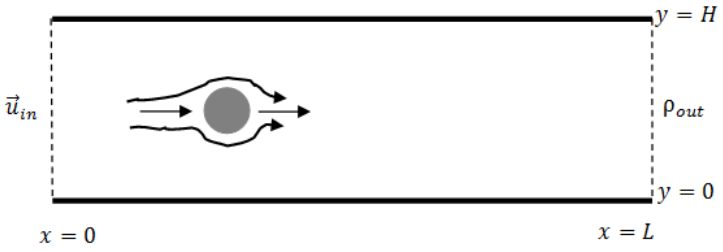

Figure 10: Illustration of flow past a cylinder

In this simulation, we set up a 2D channel with a steady Poiseuille flow. A circular cylinder is then immersed into the flow at the start of the simulation. On-grid bounce-back BCs are applied on the cylinder as well as the top and the bottom plates. Zou-He velocity and pressure (density) BCs are implemented at the inlet and the outlet of the flow (see Figure 10).

Simulations with $Re = 5, 40, 150$ have been carried out and the behavior of the flow is matched with images from laboratory experiments. The results are summarized in the following figures.

- $Re < 5$: a smooth laminar flow across the cylinder

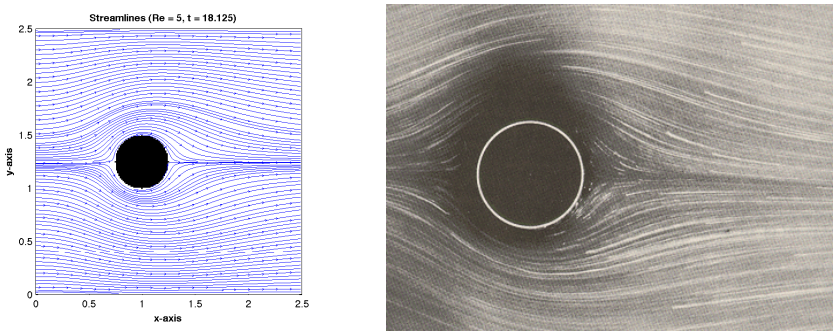

Figure 11: $Re = 5$: Laminar flow past a cylinder: simulation vs experiment

- $5 < Re < 40$: a pair of fixed symmetric vortices generated at the back of the cylinder

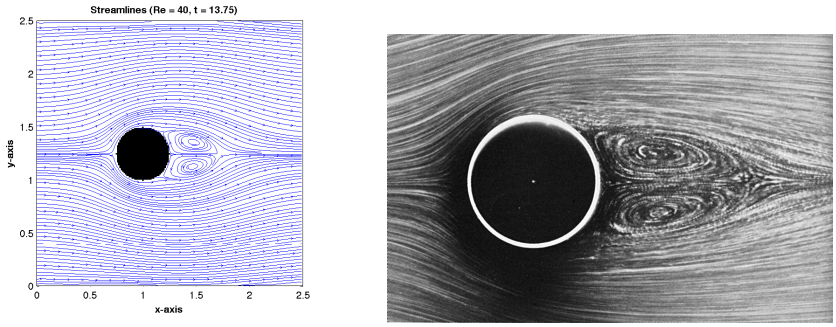

Figure 12: $Re = 40$: A fixed pair of vortices: simulation vs experiment

- $40 < Re < 400$: Vortex streets

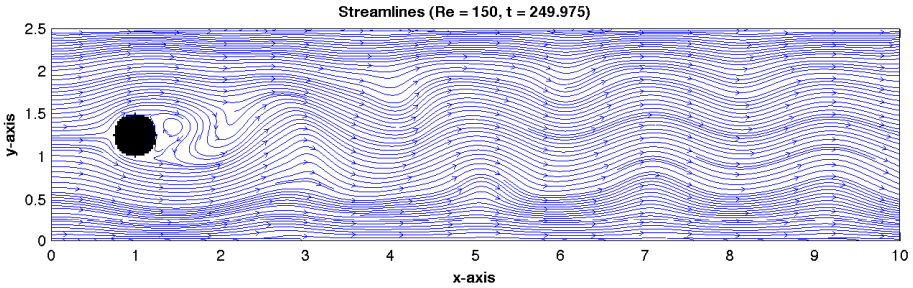

Figure 13: Streamlines of flow at $Re = 150$

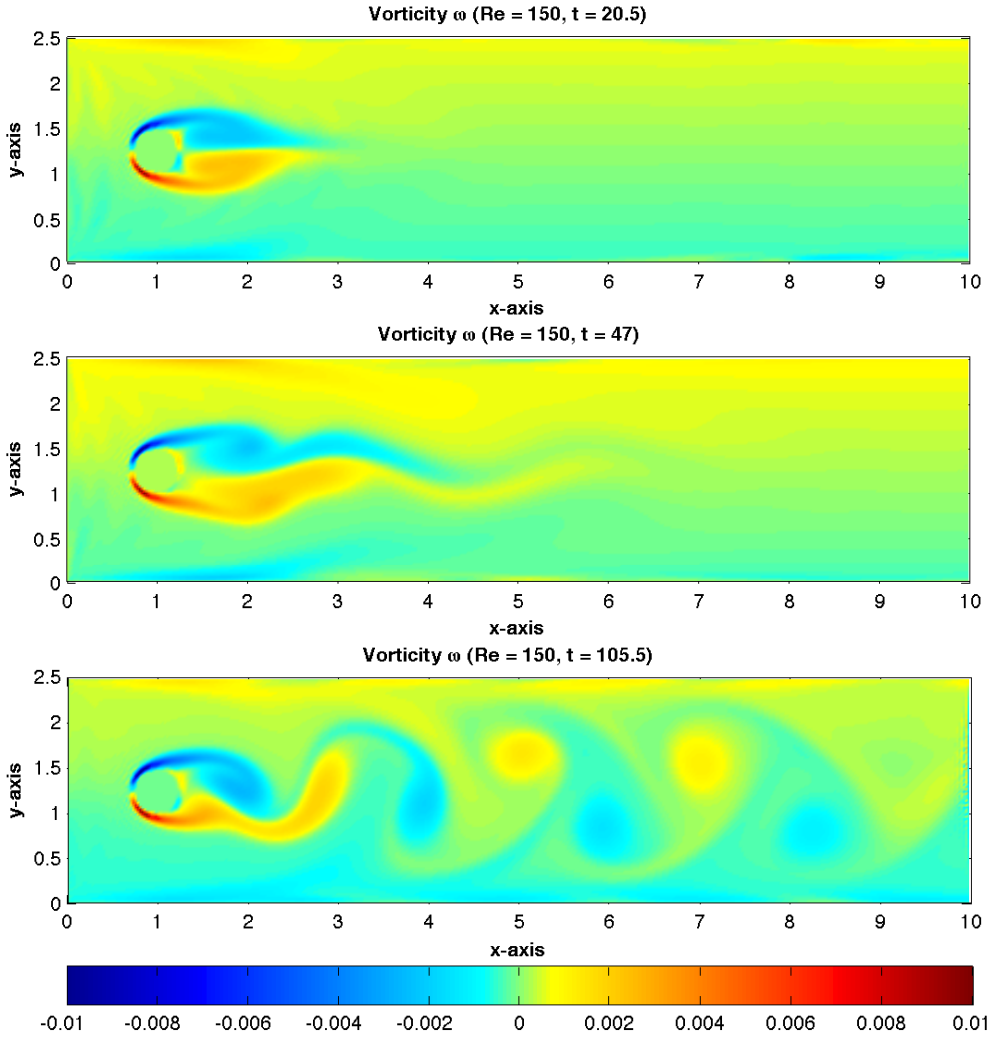

Figure 14: Vorticity plot of flow past a cylinder at $Re = 150$, a Karman vortex street is generated

7 Rayleigh-Bénard convection

Rayleigh-Bénard convection is a type of natural convection, in which the fluid motion is not purely driven by an external force, but also by density differences in the fluid due to temperature gradients. A very important implication of convection is the ocean-atmosphere dynamics, where heated air or water vapor upwell from the ocean into the atmosphere and this is fundamental in understanding climate patterns such as El Niño and La Niña.

The *Boussinesq approximation* is often used in the study of natural convection. With this approximation, density is assumed to be constant except for the buoyancy term in the equations of motion. The governing equations are

$$\nabla \cdot \vec{u} = 0 \tag{22}$$

$$\frac{D\vec{u}}{Dt} = -\frac{1}{\rho_0}\nabla p + \nu\nabla^2\vec{u} + \frac{\rho}{\rho_0}\vec{g} \tag{23}$$

$$\frac{DT}{Dt} = \kappa\nabla^2 T \tag{24}$$

where $\vec{u}$ is the fluid velocity, ν is the kinematic viscosity, ρ is the density variation, ρ_0 is the constant ambient fluid density, T is the temperature and κ is the thermal diffusivity constant. Furthermore the density ρ is assumed to be linearly related to the temperature T:

$$\rho = \rho_0(1 - \beta(T - T_0)) \tag{25}$$

Here T_0 is the average fluid temperature and β is the coefficient of thermal expansion.

By putting (25) into (23) and absorbing the first term of ρ into the pressure term, we get the following coupled equations between velocity and temperature:

$$\nabla \cdot \vec{u} = 0 \tag{26}$$

$$\frac{D\vec{u}}{Dt} = -\frac{1}{\rho_0}\nabla p + \nu\nabla^2\vec{u} - \vec{g}\beta(T - T_0) \tag{27}$$

$$\frac{DT}{Dt} = \kappa\nabla^2 T \tag{28}$$

An important observation is that T appears as a buoyancy force in the momentum equation (27). Thus the Boussinesq equations (26)-(28) can be simulated by two independent BGK models with a buoyancy forcing term coupling the two models. For velocity $\vec{u}$, a modified BGK model (ID2Q9) with much less compressible effects is applied in [6]. This model is based on the same D2Q9 lattice but uses pressure p instead of density ρ as a primitive variable. A new microscopic distribution function $g_i(\vec{x}, t)$ is introduced along with its equilibrium distribution function $g^{eq}(\vec{x}, t)$ defined by

$$g^{eq}(\vec{x}, t) = \begin{cases} -4\sigma\dfrac{p}{c^2} + s_1(\vec{u}) & i = 0 \\ \lambda\dfrac{p}{c^2} + s_i(\vec{u}) & i = 1, 2, 3, 4 \\ \gamma\dfrac{p}{c^2} + s_i(\vec{u}) & i = 5, 6, 7, 8 \end{cases} \tag{29}$$

where $s_i(\vec{u})$ is defined as before in (7).

The evolution equation of the distribution function $g_i(\vec{x}, t)$ is similar to (5),

$$g_i(\vec{x} + c\vec{e_i}\Delta t, t + \Delta t) = g_i(\vec{x}, t) - \frac{1}{\tau}(g_i - g_i^{eq}) \tag{30}$$

The relaxation time τ is related to kinematic viscosity ν through

$$\nu = \frac{2\tau - 1}{6}\frac{(\Delta x)^2}{\Delta t} \tag{31}$$

The marcoscopic velocity $\vec{u}$ and pressure p are given by

$$\vec{u} = \sum_{i=0}^{8} c\vec{e_i}g_i, \quad p = \frac{c^2}{4\sigma}\left[\sum_{i=1}^{8} g_i + s_0(\vec{u})\right] \tag{32}$$

It can be shown rigorously that the incompressible Navier-Stokes equation can be derived from this discrete model using a multiscaling expansion with an error of $O(\Delta t^2)$ [1].

A simple D2Q4 BGK model is used to simulate the advection-diffusion of temperature. A lattice with four discrete velocity directions $\vec{e_1}$, $\vec{e_2}$, $\vec{e_3}$ and $\vec{e_4}$ as defined in (2) is implemented. The evolution equations of the temperature distribution function T_i is given by

$$T_i(\vec{x} + c\vec{e_i}\Delta t, t + \Delta t) = T_i(\vec{x}, t) - \frac{1}{\tau'}(T_i - T_i^{eq}) \tag{33}$$

with the equilibrium temperature

$$T_i^{eq} = \frac{T}{4}\left[1 + 2\frac{\vec{e_i} \cdot \vec{u}}{c}\right] \tag{34}$$

The relaxation time τ' is related with the thermal diffusivity κ through

$$\kappa = \frac{2\tau' - 1}{4}\frac{(\Delta x)^2}{\Delta t} \tag{35}$$

The fluid temperature is then calculated from the temperature distribution function

$$T = \sum_{i=1}^{4} T_i \tag{36}$$

It is shown that this model is able to approximate the advection-diffusion equation (28) to $O(\Delta t^2)$ in [6].

The coupling of the two models is established by recognizing that temperature is incorporated into (27) as a buoyancy forcing term. In the discrete lattice model, this forcing term is given by:

$$b_i = -\frac{1}{2c}\Delta t \alpha_i \vec{e_i} \cdot \vec{g}\beta(T - T_0) \tag{37}$$

where $\alpha = \delta_{i2} + \delta_{i4}$ and δ_{ij} is the Kronecker delta.

By adding this force term (37) to the evolution equation (30), we complete the coupling of the two BGK models:

$$g_i(\vec{x} + c\vec{e_i}\Delta t, t + \Delta t) = g_i(\vec{x}, t) - \frac{1}{\tau}(g_i - g_i^{eq}) + b_i \tag{38}$$

The configuration of Rayleigh-Bénard convection is a 2D rectangular container with a hot wall on the bottom and a cool wall on the top (see Figure 15).

There are two dimenstionless constants that characterize the type of heat transfer.

- The Rayleigh number $Ra = g\beta\Delta T H^3/(\nu\kappa)$, where $\Delta T = T_h - T_c$ is the temperature gradient and H is the height of the domain. Heat transfer primarily takes the form of conduction for Ra below a critical value. On the other hand, convection of thermal energy dominates for Ra above a critical value.
- The Prantl number $Pr = \nu/\kappa$ controls the relative thickness of the momentum and thermal boundary layers.

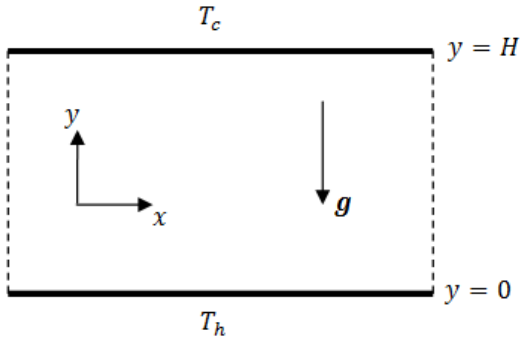

Figure 15: Illustration of Rayleigh-Bénard convection

In all simulations, a bounce-back (no-slip) boundary condition for velocity and a Zou-He boundary condition for temperature are applied on the top and the bottom wall. Periodic boundary conditions for both velocity and temperature are applied on the two vertical walls. The lattice size is chosen to be 50×200. ν, κ and τ' are subsequently determined by fixing τ, Ra and Pr. In the first two simulations, we fix $\tau = 1/1.2$, $Pr = 0.71$ for air and compare the results of $Ra = 5 \times 10^3$ and 5×10^4.

At the start of the simulation, thermal energy is primarily transferred in conduction due to a temperature gradient between the two walls. As the density of the fluid near the bottom wall decreases, the buoyancy force will take over and the less dense hot fluid upwells and carries the heat along with it. The hot fluid loses heat and becomes more dense as it encounters colder fluid. Once the buoyancy force is no longer dominant, the fluid then takes a downward motion. This process is best illustrated by looking at the convection streamlines and the temperature figure. It is interesting to point out that the stability of convection cells changes with varying Ra (see Figure 16 and 17).

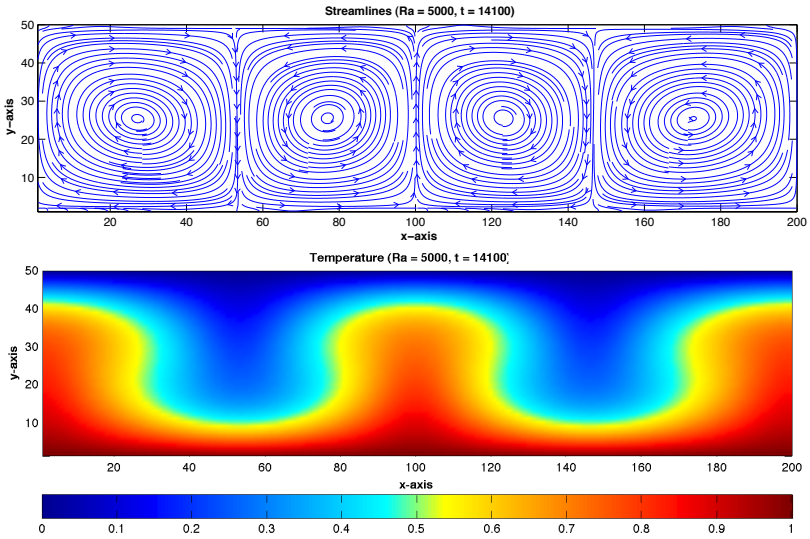

Figure 16: Streamlines of convection and temperature field at $Ra = 5 \times 10^3$

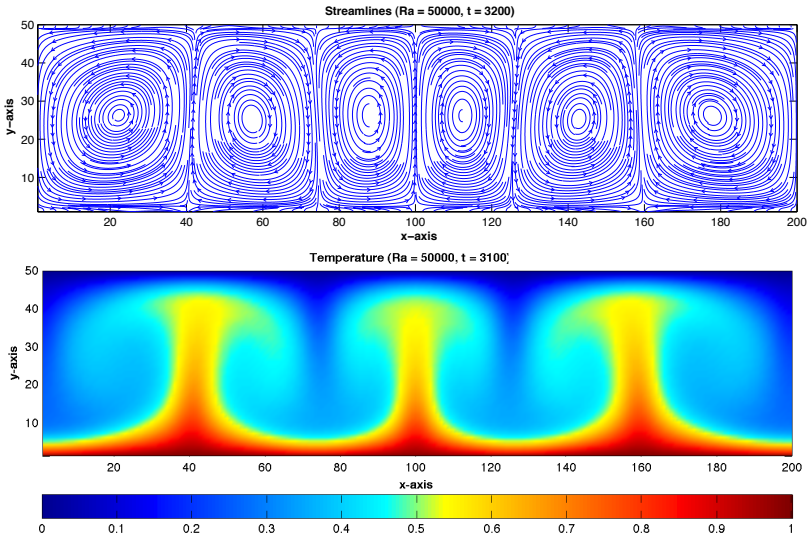

Figure 17: Streamlines of convection and temperature field at $Ra = 5 \times 10^4$

For the last simulation, a very high Rayleigh number $Ra = 10^7$ is used. However, τ is set to be 1/1.95 without running into numerical instability. The structure of the the convection cell is much more complicated and the temperature field suggests that it is close to turbulence.

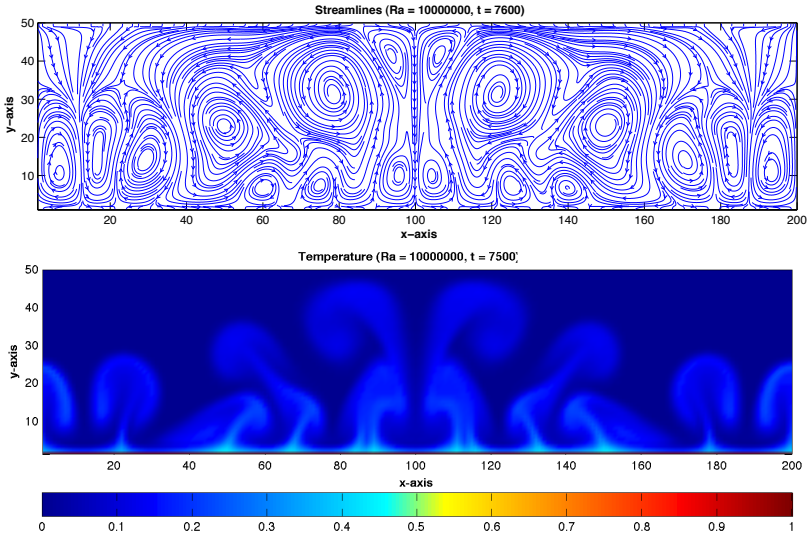

Figure 18: Streamlines of flow and temperature field at $Ra = 10^7$

8 Connection with FD and the Navier-Stokes Equations

The Lattice Boltzmann method can be viewed as a special finite difference method [7] for solving the Boltzmann transport equation (1) on a lattice. To see this, we write down the Boltzmann transport equation in terms of the discrete distribution function,

$$\frac{\partial f_i}{\partial t} + \vec{e}_i \cdot \nabla f_i = \Omega_i \tag{39}$$

If we discretize the differential operator and the collision operator in this form,

$$\frac{f_i(\vec{x}, t+\Delta t) - f_i(\vec{x}, t)}{\Delta t} + \frac{f_i(\vec{x}+\vec{e}_i\Delta x, t+\Delta t) - f_i(\vec{x}, t+\Delta t)}{\Delta x} = -\frac{f_i(\vec{x}, t) - f_i^{eq}(\vec{x}, t)}{\tau} \tag{40}$$

and assume that $\Delta x = \Delta t = 1$, we essentially recover the LBM evolution equation (5).

The primary reason why LBM can serve as a method for fluid simulations is that the Navier-Stokes equations can be recovered from the discrete equations through the Chapman-Enskog procedure, a multi-scaling expansion technique. Specifically the ID2Q9 model used in simulating Rayleigh-Bénard convection is able to recover the incompressible Navier-Stokes equations. Here we highlight the key steps. A detailed derivation is provided in the appendix of [1, 8].

With a multi-scaling expansion, we may write

$$g_i = g_i^{(0)} + \epsilon g_i^{(1)} + \epsilon^2 g_i^{(2)} + \dots \tag{41}$$

$$\frac{\partial}{\partial t} = \epsilon \frac{\partial}{\partial t_1} + \epsilon^2 \frac{\partial}{\partial t_2} + \dots \tag{42}$$

$$\frac{\partial}{\partial x} = \epsilon \frac{\partial}{\partial x_1} \tag{43}$$

where $g_i^{(0)} = g_i^{eq}$ and $\epsilon = \Delta t$ is the expansion parameter. It is proved in [6] that up to $O(\epsilon)$ we can derive the following continuity and momentum equations,

$$\nabla \cdot \vec{u} = 0 + O(\epsilon) \tag{44}$$

$$\frac{\partial \vec{u}}{\partial t} + \nabla \cdot (\mathbf{\Pi^0}) = 0 + O(\epsilon) \tag{45}$$

where $\mathbf{\Pi^0}$ is the equilibrium flux tensor. And to $O(\epsilon^2)$, the following equations are derived

$$\nabla \cdot \vec{u} = \epsilon \left(\tau - \frac{1}{2}\right) \mathbf{P} + O(\epsilon^2) \tag{46}$$

$$\frac{\partial \vec{u}}{\partial t} + \nabla \cdot (\mathbf{\Pi^0}) = \epsilon \left(\tau - \frac{1}{2}\right) \mathbf{Q} + O(\epsilon^2) \tag{47}$$

where it is shown that $\mathbf{P} \sim O(\epsilon)$ and $\mathbf{Q} \sim O(\epsilon) + O(M^2) + \frac{c^2}{3}\nabla^2 \vec{u}$, M is the Mach number. By applying results of $\mathbf{P}$ and $\mathbf{Q}$ to (46) and (47), the continuity equation is derived accurate to $O(\epsilon^2)$ and the momentum equation is derived to $O(\epsilon^2 + \epsilon M^2)$.

$$\nabla \cdot \vec{u} = 0 + O(\epsilon^2) \tag{48}$$

$$\frac{\partial \vec{u}}{\partial t} + \vec{u} \cdot \nabla \vec{u} = -\nabla p + \nu \nabla^2 \vec{u} + O(\epsilon^2 + \epsilon M^2) \tag{49}$$

9 Conclusion

In this project, we conducted a comprehensive study of the Lattice Boltzmann method and its corresponding boundary conditions. The validity of this method was verified by comparing numerical solutions to the exact solutions of the steady plane Poiseuille flow. Three nontrivial simulations: lid-driven cavity flow, flow past a circular cylinder and Rayleigh-Bénard convection were performed and they agreed closely with physical situations. We drew a connection between LBM and FD and concluded that it is a special discretization of the Boltzmann transport equation. The connection between LBM and Navier-Stokes was not fully worked out in this report, though we did attempt to highlight the important steps.

The Lattice Boltzmann method has several advantages for fluid simulations over traditional finite difference methods.

- LBM is very applicable to simulate multiphase/multicomponent flows.
- Complex boundaries are much easier to deal with using on-grid bounce-back and thus LBM can be applied to simulate flows with complex geometries such as porous media flows.
- LBM can be easily parallelized and thus can be applied to do large simulations.

However, by reading references on the derivation of the Navier-Stokes equations from LBM, we realize that this method is subject to some compressible effects. Therefore it is expected that some source of errors come in the form of artificial compressibility when solving the incompressible Navier-Stokes equations using LBM.

References

[1] Z. Guo, B. Shi, and N. Wang, *Lattice BGK Model for Incompressible Navier-Stokes Equation*, J. Comput. Phys. **165**, 288-306 (2000)

[2] M. Sukop and D.T. Thorne, *Lattice Boltzmann Modeling: an introduction for geoscientists and engineers*. Springer Verlag, 1st edition. (2006)

[3] R. Begum, and M.A. Basit, *Lattice Boltzmann Method and its Applications to Fluid Flow Problems*, Euro. J. Sci. Research **22**, 216-231 (2008)

[4] S. Succi, *The Lattice Boltzmann Equation for Fluid Dynamics and Beyond*. pp. 82-84 Oxford University Press, Oxford. (2001)

[5] Q. Zou, and X. He, *Pressure and velocity boundary conditions for the lattice Boltzmann*, J. Phys. Fluids **9**, 1591-1598 (1997)

[6] Z. Guo, B. Shi, and C. Zheng, *A coupled lattice BGK model for the Boussinesq equations*, Int. J. Numer. Meth. Fluids **39**, 325-342 (2002)

[7] S. Chen, D. Martínez, and R. Mei, *On boundary conditions in lattice Boltzmann methods*, J. Phys. Fluids **8**, 2527-2536 (1996)

[8] X. He, L. Luo, *Lattice Boltzmann for the incompressible Navier-Stokes equation*, J. Stat. Phys, Vol 88, Nos. 3/4 (1997)